APPLIED GEOPHYSICS, Vol.15, No.2 (June 2018), P. 280–289, 9 Figures.
DOI:10.1007/s11770-018-0682-9

# Identification of blasting vibration and coal-rock fracturing microseismic signals*

Zhang Xing-Li*[1,2], Jia Rui-Sheng[1,2], Lu Xin-Ming[1,2], Peng Yan-Jun[1,2], and Zhao Wei-Dong[1,2]

**Abstract**: A new method based on variational mode decomposition (VMD) is proposed to distinguish between coal-rock fracturing and blasting vibration microseismic signals. First, the signals are decomposed to obtain the variational mode components, which are ranked by frequency in descending order. Second, each mode component is extracted to form the eigenvector of the energy of the original signal and calculate the center of gravity coefficient of the energy distribution plane. Finally, the coal-rock fracturing and blasting vibration signals are classified using a decision tree stump. Experimental results suggest that VMD can effectively separate the signal components into coal-rock fracturing and blasting vibration signals based on frequency. The contrast in the energy distribution center coefficient after the dimension reduction of the energy distribution eigenvector accurately identifies the two types of microseismic signals. The method is verified by comparing it to EMD and wavelet packet decomposition.

**Keywords**: Coal-rock fracturing microseismic, blasting vibration, variational mode decomposition, signal identification

## Introduction

In recent years, the real-time, continuous, and online microseismic monitoring of rocks in coal mines has advanced considerably. The mining environment is complex owing to the background noise, blasting vibrations, etc. Such noise prevents the accurate recording of microseismic activity. In addition, highly knowledgeable personnel are required to manually identify the microseismic events. The combination of these factors affects the efficiency of the various monitoring systems. Blasting operations are common in coal mines, and the waveforms of rock fracturing and blasting vibrations are very similar, resulting in processing errors.

Presently, the identification of microseismic signals is mainly based on time–frequency analysis and parameter identification. The most commonly used time–frequency methods are the Fourier transform, the wavelet transform, the wavelet packet transform, the frequency

Manuscript received by the Editor October 3, 2017; revised manuscript received April 28, 2018.
*This work was supported by the National Key Research and Development program of China (No. 2016YFC0801406), Shandong Key Research and Development program (Nos. 2016ZDJS02A05 and 2018GGX109013) and Shandong Provincial Natural Science Foundation (No. ZR2018MEE008).
1. College of Computer Science and Engineering, Shandong University of Science and Technology, Qingdao 266590, China.
2. Shandong Province Key Laboratory of Wisdom Mine Information Technology, Shandong University of Science and Technology, Qingdao 266590, China.
♦Corresponding author: Zhang Xing-Li (Email: xlzhang_only@163.com)

slice wavelet transform, and the empirical mode decomposition (EMD). Lu et al. (2005) used the Fourier transform to analyze the power spectrum and amplitude frequency of roof-pressure relief-blasting microseismic signals, and coal-seam pressure-blasting microseismic signals, and preliminarily identified the different types of microseismic signals in mines. However, the Fourier transform is traditionally used to analyze periodic stationary signals and has not been found effective for random nonstationary microseismic signals with spikes and mutations (Alvanitopoulos et al., 2012; Gaci, 2014). Wavelet analysis simultaneously analyzes time and frequency analyses (Tang et al., 2011). However, this type of analysis requires to choose a suitable wavelet base (Zhu et al., 2012a; Jiang et al., 2014) to improve decomposition. For example, the wavelet energy spectrum coefficient has been used to analyze the energy distribution characteristics of rock fracturing and noise signals. Presently, many have applied wavelet analysis to the waveforms of natural earthquakes (Liu et al., 2003; Allmann et al., 2008; Huang et al., 2010) and microseismic signals in mines (Zhu et al., 2012b). The empirical mode decomposition, proposed by Huang et al. (1998), detects and decomposes a signal into principal modes. This method has been proven suitable for handling random nonstationary signals and it has been applied to noise reduction in mine microseismic signals (Jia et al., 2015), feature extraction (Wu et al., 2014), and classification (Shang et al., 2016; Jia et al., 2017). However, the boundary effects and modal aliasing in the EMD method (Dong et al., 2016; Zhang et al., 2018) affect the decomposition results, causing instability and nonuniqueness. Thus, EMD cannot be used to effectively identify signals. Parameter identification uses linear regression (Zhao et al., 2015; Ma et al., 2015) to extract the slope of the starting-up trend line and the coordinates of the first and maximum peaks. Then, the identification model is established by applying Fisher discriminant analysis. However, this requires a high signal waveform, which affects the signal identification. Many have proposed to identify microseismic waves through coal seams and rocks by using the arrival time of the seismic waves but the error (Allen, 1978) in window selection, and signal-to-noise ratio (Akaike, 1987; Wang, 2018) is high.

Variational mode decomposition is an entirely nonrecursive decomposition model, in which the modes are extracted concurrently (Konstantin and Dominique, 2014). The method searches for ensembles of modes and their respective central frequencies, in which the modes collectively reproduce the input signal, while each mode turns into a baseband after demodulation. VMD overcomes the boundary effects and modal aliasing in the EMD and other recursive decomposition algorithms, and selects the wavelet base functions in wavelet or wavelet packet analysis much easier. Presently, VMD has been applied to the functional coupling analysis of electroencephalograms and electromyograms (Xie et al., 2016), fault identification (Tang and Wang, 2015), and imaging (Zhang et al., 2016). To tackle the identification of rock fracturing and blasting vibration, we use the VMD to study the energy distribution in each mode, along with the energy focus coefficient, and extract the energy focus coefficient as the characteristic parameter to classify and identify these two types of microseismic signals.

# Theory

## Variational mode decomposition

Variational mode decomposition (VMD) (Dragomiretskiy and Zosso, 2014) is a nonrecursive signal decomposition method. VMD decomposes the real-time input signal $x$ into K discrete subsignals (modes) $u_k(k = 1,2,\ldots,K)$ ($\{u_k\} = \{u_1, u_2, \ldots,u_K\}$; $k$ is the serial number of each mode and $K$ is the total number of modes. Each mode has a limited bandwidth with a central frequency $\omega_k(k = 1,2,\ldots,K)$. The constraints are that the sum of the bandwidth of all modes is the smallest and the sum of all modes is equal to the input signal $x$. VMD addresses the constrained problem in different ways. It has been suggested to use both a quadratic penalty term $\alpha$ and Lagrangian multipliers $\lambda$ to make the problem unconstrained. The alternating direction method of multipliers was used to obtain the optimal solution of the constrained variational model, and the input signal was decomposed into each mode and its central frequency.

The steps in VMD were as follows:

Input: original signal $x$ and total number of modes $K$;

Output: $K$ modes.

Step 1: initialize each mode $\left\{\hat{u}_k^1\right\}$, central frequency $\left\{\hat{\omega}_k^1\right\}$, and Lagrangian multipliers $\hat{\lambda}^1$, $n = 0$;

Step 2: $n = n + 1$, update $u_k$ and $\omega_k$ according to equations (1) and (2) (Dragomiretskiy and Zosso, 2014)

$$\hat{u}_k^{n+1}(\omega) = \frac{\hat{x}(\omega) - \sum_{i<k}\hat{u}_i^{n+1}(\omega) - \sum_{i>k}\hat{u}_i^{n}(\omega) + \frac{\hat{\lambda}^n(\omega)}{2}}{1 + 2\alpha(\omega - \omega_k^n)^2}, \quad (1)$$

$$\omega_k^{n+1} = \frac{\int_0^\infty \omega \left|\hat{u}_k^{n+1}(\omega)\right|^2 d\omega}{\int_0^\infty \left|\hat{u}_k^{n+1}(\omega)\right|^2 d\omega}. \quad (2)$$

Step 3: update $\lambda$ according to equation (3) (Dragomiretskiy and Zosso, 2014)

$$\hat{\lambda}^{n+1}(\omega) = \hat{\lambda}^n(\omega) + \tau(\hat{x}(\omega) - \sum_k \hat{u}_k^{n+1}(\omega)), \quad (3)$$

where $\tau$ is the update step of the Lagrangian multiplier;

Step 4: for $\varepsilon = 0$, if the condition

$$\sum_k (\left\|\hat{u}_k^{n+1} - \hat{u}_k^n\right\|_2^2 / \left\|\hat{u}_k^n\right\|_2^2) < \varepsilon$$

(Dragomiretskiy and Zosso, 2014) is satisfied then stop the iteration and output the $K$ modes are output; otherwise, go back to step 2.

In general, VMD is a powerful signal decomposition method in the frequency domain that can tackle modal aliasing better. We use VMD to decompose the two kinds of vibration signals and accurately calculate the band energy of the signal frequency and extract the energy eigenvectors.

## Energy characterization of the signals

The original signal $x(t)$ is decomposed and the $K$ modes are $\{u_1, \ldots, u_k, \ldots, u_K\}$. The energy $E_k$ of mode $u_k(t)$ is computed as follows:

$$E_k = \int \left|A_k(t)\right|^2 dt = \sum_{i=1}^{N} \left|x_{ki}\right|^2, \quad (4)$$

where $x_{ki}$ ($k$ = 1,2, …, $K$; $i$ = 1,2, …, $N$) is the discrete point amplitude of the k-th mode component $u_k$, $N$ is the number of sampling points in the original signal, and $K$ is the total number of modes.

The total energy $E$ of the original signal $x(t)$ is

$$E = \sum_{k=1}^{K} E_k. \quad (5)$$

The normalized energy of each mode is

$$P(k) = \frac{E_k}{E}. \quad (6)$$

## Energy focus coefficient

In a gravitational field, the center of gravity is the average location of the weight of an object. In the energy distribution plane, the energy center is the focal point of energy. The energy distribution in rock fracturing and blasting vibrations are significantly different; thus, there are also differences in the position of the energy center of these microseismic signals. To facilitate data processing and improve the effectiveness of the final classification, the energy focus coefficient of the energy distribution was obtained after the dimension reduction of the energy eigenvectors. In this study, the two kinds of microseismic signals are classified and identified based on the energy focus coefficient of the energy distribution.

The normalized energy of each mode was first calculated. Next, the energy distribution vector $P$ was obtained, where $P = (P(1), \ldots, P(k), \ldots, P(K))$, and the energy distribution plane was constructed. In the energy distribution plane, the mode number $k$ was chosen as the X-axis and the normalized energy $P(k)$ corresponding to $k$ was the Y-axis.

The energy focus coefficient on the X-axis $C_x$ ($0 < C_x \leq 1$) is

$$C_x = \frac{\sum_{i=1}^{K} (i \cdot P(i))}{K \cdot \sum_{i=1}^{K} P(i)}, \quad (7)$$

$C_x$ describes the of signal energy in the plane of energy distribution. When $0 < C_x \leq 0.5$, the signal energy is concentrated in the first three high-frequency components, which can be initially determined as blasting vibration signals. When $0.5 < C_x \leq 1$, the signal energy focuses on the late three low-frequency components, which can be initially determined as coal-rock fracturing microseismic signals.

# Experiments

Coal-rock fracturing microseismic and blasting vibration data were selected from a coal mine, part of the Linkuang Group. The mine roof is dominated by mudstone and sandy mudstone, and locally siltstone. The mine floor consists of mudstone, followed by siltstone, and is characterized by more fractures and rock mass of poor stability. The blasting technique used in the mine is microdifferential blasting.

## Energy distribution of the two types of microseismic signals

To compare the energy characteristics of rock

fracturing and blasting vibration signals, the two types of microseismic signals were selected and decomposed by the VMD method, and six modes were obtained, respectively. Then, the energy of the microseismic signals for the different modes was analyzed. The waveform and time–frequency relation of the coal-rock fracturing and blasting vibration signals are shown in Figures 1 and 2.

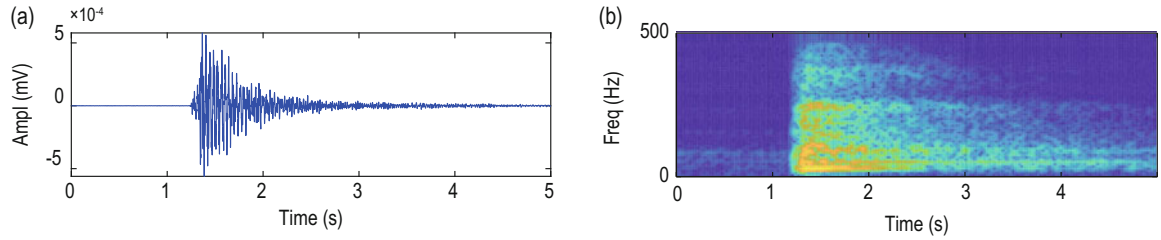


**Fig.1 Coal-rock fracturing microseismic signal: (a) waveform; (b) time vs frequency.**

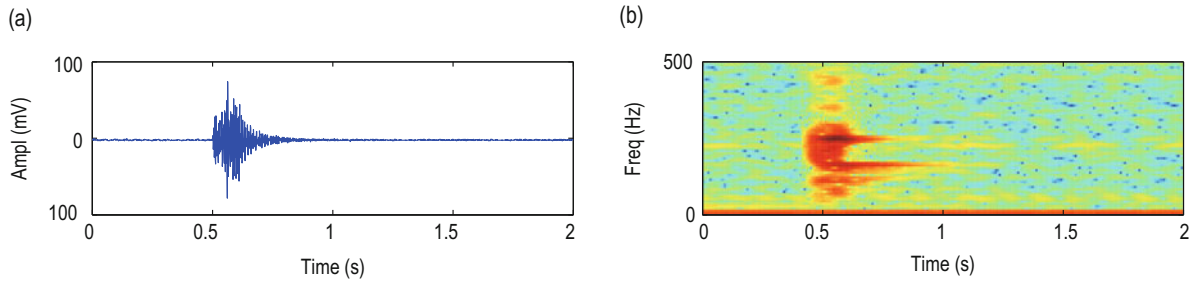


**Fig.2 Blasting vibration microseismic signal: (a) waveform; (b) time vs frequency.**

Figures 1a and 2a show that the rock fracturing and blasting vibration waveforms are very similar and are very difficult to distinguish visually. However, the energy distributions of rock fracturing and blasting vibration signals differ greatly. As shown in Figure 1b, the energy distribution of the rock fracturing signal is between 0 Hz and 200 Hz, and the main energy is between 20 Hz and 100 Hz. In Figure 2b, the energy distribution of the blasting vibration signal is between 50 Hz and 300 Hz and the main energy is between 150 Hz and 300 Hz.

The two types of microseismic signals are decomposed using the VMD method, and the waveforms and time versus frequency of each mode of the rock fracturing and blasting vibration signals are shown in Figures 3

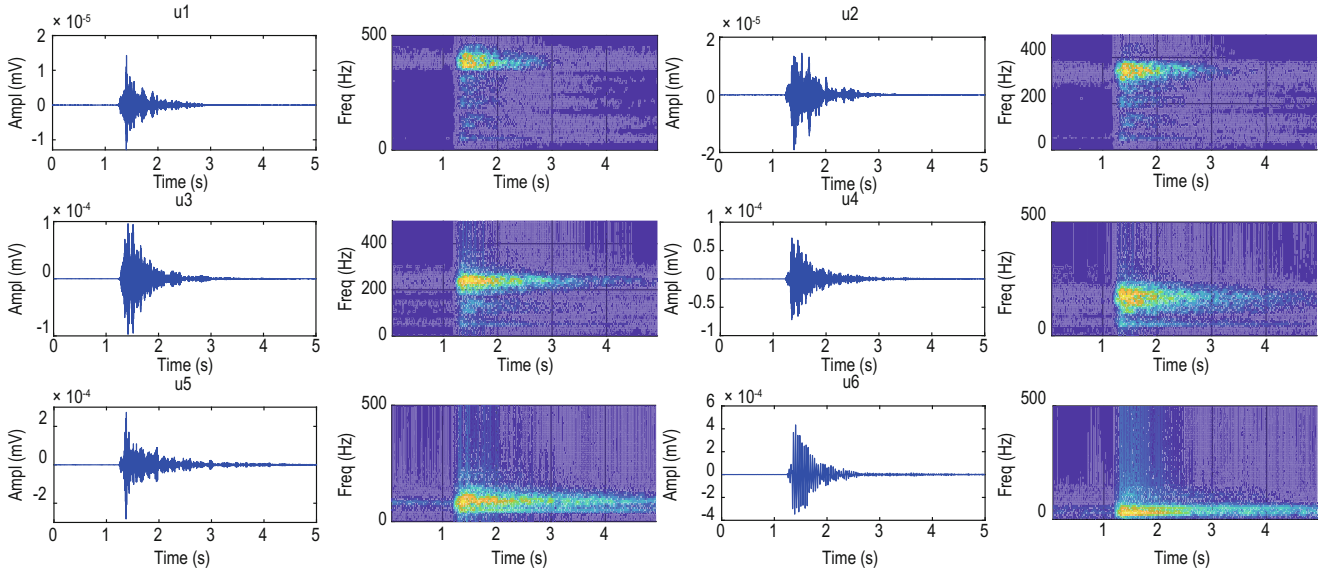


**Fig.3 VMD decomposition results for the coal-rock fracturing microseismic signal; left columns: $u_1$–$u_6$ are the waveforms of the six modes obtained by decomposition; right columns: time vs frequency.**

and 4. The VMD method decomposes each signal and its energy into six narrowband modes. No modal aliasing is observed between modes. The normalized energy of each mode is then calculated, and the energy distribution vector $P$ of the rock fracturing signal is 0.02, 0.09, 3.01, 1.45, 13.41, and 82.02. The energy distribution vector $P$ of the blasting vibration signal is 0.92, 64.93, 7.11, 15.34, 1.72, and 9.98. The distribution histograms of the two microseismic signals are shown in Figure 5.

In Figure 5a, the energy of the rock fracturing signal is mainly concentrated in the low-frequency modes and the red open circle denotes the center of the energy distribution plane of the rock fracturing signal, where $C_x$ = 0.96. In Figure 5b, the energy of the blasting vibration signal is mainly concentrated in the higher frequency modes and the red solid circle denotes the center of the energy distribution plane of the blasting vibration signal, where $C_x$ = 0.47.

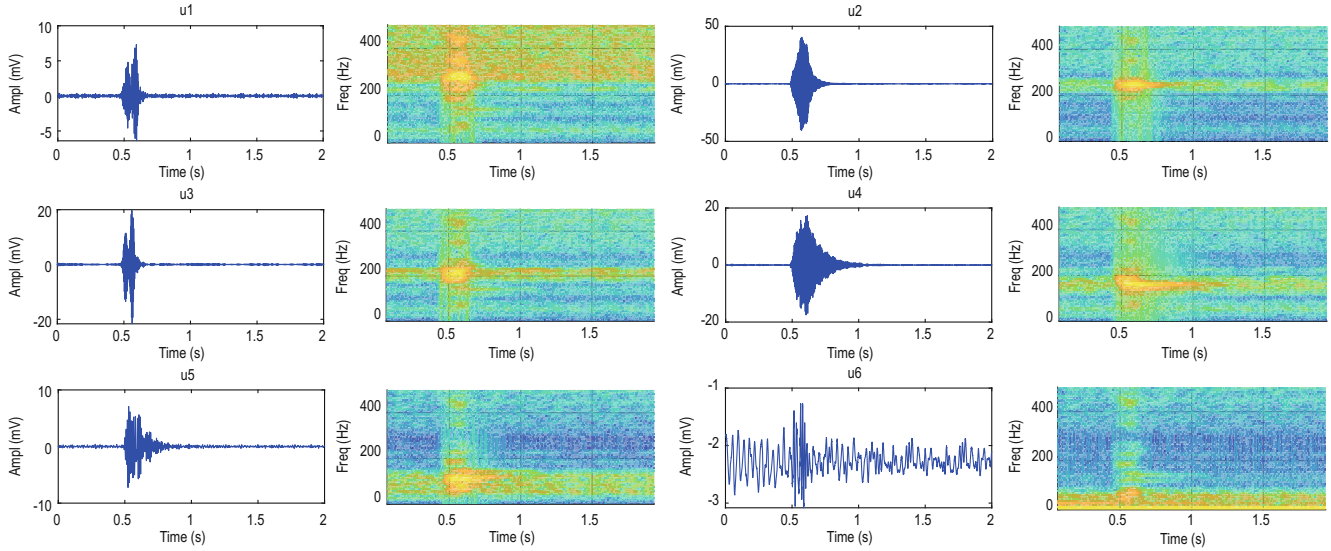


**Fig.4 VMD decomposition results for the blasting vibration signal: left columns: $u_1$–$u_6$ are the waveforms of the six modes obtained by decomposition; right columns: time vs frequency.**

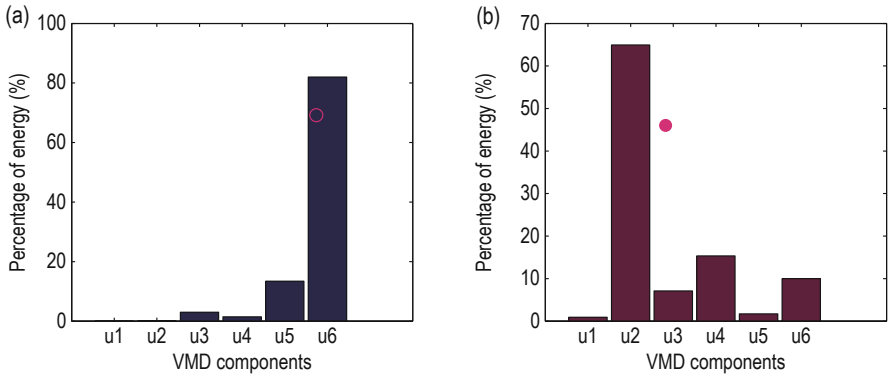


**Fig.5 Energy distribution of (a) rock fracturing and (b) blasting vibration microseismic signal.**

## Microseismic signal identification algorithm based on the VMD method

The $K$ narrowband modes with central frequencies obtained by the VMD adaptive decomposition method contain local and characteristic signals at different time scales. First, the microseismic signal was adaptively decomposed by using the VMD method and then the energy of each narrowband mode was obtained. Second, the $K$-dimensional energy eigenvector $P$ of the microseismic signal was obtained. Based on $P$, the energy distribution plane is constructed and dimension reduction is performed on the energy eigenvector $P$ to calculate the energy distribution center coefficient $C_x$ for

classifying the two types of microseismic signal.

The microseismic signal identification algorithm based on the VMD method has as follows:

Step 1: Initialization and the number of modes is set at $K = 6$;

Step 2: The input signal $x(t)$ is decomposed using the VMD method and six modes $U = \{u_1,u_2,u_3,u_4,u_5,u_6\}$ are obtained;

Step 3: Calculate $E_k$ of mode $u_k$ using equation (4);

Step 4: Calculate each mode component $P(k)$ based on equations (5) and (6), and obtain the vector $P = (P(1), P(2), P(3), P(4), P(5), P(6))$;

Step 5: Construct the energy distribution plane; calculate the energy focus coefficient of the X-axis $C_x$ with equation (7) and compare the $C_x$ and T values. If $C_x > T$, the input signal is a rock fracturing signal. If $C_x \leq T$, the input signal is a blasting vibration signal.

# VMD analysis of the microseismic signals

## Value of the $K$

The VMD method requires predefining the number of $K$ modes and the method output is sensitive to the number of modes. After decomposition, the $K$ value, and the central frequency and frequency band width of each mode change. In addition, the normalized energy of each mode has changed. If the $K$ value is small, this is due to underdecomposition. If the $K$ value is high, overdecomposition may have occurred. In general, the minimum value of $K$ is 2 and the maximum value is about 10. Therefore, to avoid the problem of under- or overdecomposition, the energy distribution of the signal with $K$ values of 2–14 is monitored to determine the most suitable value of $K$. A typical rock fracturing signal (Figure 1) is decomposed by the VMD method. The sampling frequency of the signal is 1,000 Hz, and the number of sampling points is 5,000. The normalized energy and the energy focus coefficient of each mode for different $K$ values are listed in Table 1.

When $K$ is 2, the original signal is decomposed into two modes, and the energy is distributed in two regions. When $K$ is 3 or 4, the energy is concentrated in three regions; the normalized energy of the first region is less than 1%, that of the second region is approximately 10%, that of energy of the third region is approximately 89%. Starting from a $K$ value of 5, the original signal is decomposed into $K$ modes and the energy is concentrated into four regions; the normalized energy of the first region is less than 1%, that of the second region is approximately 5%, that of the third region is approximately 15%, and that of the fourth region is approximately 79%.

**Table 1 Energy distribution and energy focus coefficients**

| $K$ | Normalized energy of each mode | | | | | | | | | | | | | | $C_x$ |
|---|---|---|---|---|---|---|---|---|---|---|---|---|---|---|---|
| | $u_1$ | $u_2$ | $u_3$ | $u_4$ | $u_5$ | $u_6$ | $u_7$ | $u_8$ | $u_9$ | $u_{10}$ | $u_{11}$ | $u_{12}$ | $u_{13}$ | $u_{14}$ | |
| 2 | 12.28 | 87.72 | - | - | - | - | - | - | - | - | - | - | - | - | 0.94 |
| 3 | 0.59 | 9.88 | 89.53 | - | - | - | - | - | - | - | - | - | - | - | 0.96 |
| 4 | 0.34 | 9.73 | 14.76 | 75.18 | - | - | - | - | - | - | - | - | - | - | 0.91 |
| 5 | 0.12 | 1.78 | 1.39 | 13.55 | 83.15 | - | - | - | - | - | - | - | - | - | 0.96 |
| 6 | 0.02 | 0.09 | 3.04 | 1.53 | 13.20 | 82.12 | - | - | - | - | - | - | - | - | 0.96 |
| 7 | 0.02 | 0.14 | 0.37 | 2.35 | 2.07 | 12.61 | 82.45 | - | - | - | - | - | - | - | 0.95 |
| 8 | 0.01 | 0.12 | 0.08 | 3.48 | 1.88 | 4.06 | 10.92 | 79.45 | - | - | - | - | - | - | 0.95 |
| 9 | 0.01 | 0.05 | 0.12 | 0.22 | 3.37 | 1.96 | 9.57 | 14.88 | 69.81 | - | - | - | - | - | 0.94 |
| 10 | 0.00 | 0.02 | 0.13 | 0.07 | 2.89 | 1.30 | 1.66 | 13.72 | 18.19 | 62.03 | - | - | - | - | 0.93 |
| 11 | 0.00 | 0.02 | 0.12 | 0.09 | 0.15 | 3.78 | 1.75 | 1.94 | 17.15 | 20.64 | 54.35 | - | - | - | 0.92 |
| 12 | 0.00 | 0.02 | 0.07 | 0.10 | 0.05 | 1.96 | 1.55 | 1.83 | 2.06 | 19.34 | 24.22 | 48.79 | - | - | 0.92 |
| 13 | 0.00 | 0.01 | 0.02 | 0.11 | 0.07 | 0.12 | 3.84 | 1.21 | 1.54 | 2.91 | 18.82 | 28.41 | 42.93 | - | 0.91 |
| 14 | 0.01 | 0.00 | 0.01 | 0.11 | 0.08 | 0.04 | 1.20 | 2.22 | 1.55 | 1.52 | 4.94 | 16.68 | 33.35 | 38.30 | 0.91 |

The number of mode components for 5% normalized energy versus $K$ is shown in Figure 6a. As it can be seen from Figure 6a, with increasing $K$, the number of mode components with normalized energy less than 5% is also increasing. Owing to the increase in $K$, the energy distribution is decomposed in the first and second

regions, whereas the total energy distribution in the third and fourth regions does not significantly change. With increasing $K$, overdecomposition occurs in the low-frequency region. In Figure 6b, $K$ has little effect on the energy distribution center coefficient. Considering the complexity of the algorithm, the higher the decomposition level is, the higher the complexity of the algorithm will be. Therefore, by considering the above three aspects, $K$ is set at 6.

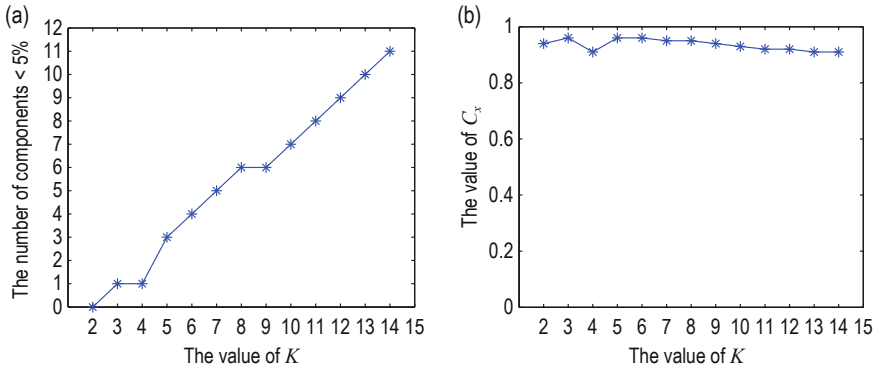


**Fig.6 (a) Number of mode components for 5% normalized energy and (b) energy focus coefficient vs $K$.**

## Threshold value

The threshold has been found to affect the classification results and accuracy. In this study, a machine learning algorithm, which is referred to as the decision stump method, was used to solve the two types of classification. The decision stump method is a linear classifier. First, the threshold Tini is estimated and then it is updated according to the training data. Finally, the best optimal threshold Tbest with the least misclassification errors is obtained as the threshold of the decision stump.

In this study, the energy focus coefficient $C_x$ was used for identification purposes and the microseismic signals were classified as labels. For $Y = 1$, the microseismic signal is a rock fracturing signal and, for $Y = 0$, the microseismic signal is a blasting vibration signal. The model function of the decision stump is $f(C_x) = (C_x – T_{ini})$, where $T_{ini}$ is the initial threshold, and when $f(C_x) > 0$, then $Y = 1$ or $Y = 0$. The simplest linear search algorithm for Tbest has as follows:

Input: energy focus coefficient $C_x$, label $Y$, and learning step $L_B$;

Output: optimal Tbest;

Step 1: initialization begins with $T_{ini} = \min(C_x)$, $T_{best} = T_{ini}$, $L_B = 0.01$, $minErr = 99999$;

Step 2: $numErr$= numberOfErrors($T_{ini}$);

Step 3: if $numErr \leq minErr$, then $minErr = numErr$, $T_{best} = T_{ini}$ end if;

Step 4: $T_{ini} = T_{ini} + L_B$, repeat the second and third steps until $T_{ini} = \max(C_x)$ and end the loop. Tbest is the output.

In the above, $minErr$ is an intermediate variable that is used to store the minimum number of misclassification errors. The function numberOfErrors ($T_{ini}$) is used to count the number of errors where Tini is the threshold. After searching for $C_x$ from $T_{ini} = \min(C_x)$ to $T_{ini} = \max(C_x)$, the least error Tbest is obtained as the optimal threshold for the decision tree stumps.

## Experiment and analysis

In this study, 15 sets of coal-rock fracturing signals and 15 sets of blasting vibration signals were selected for training and decomposed using the VMD method. The normalized energy of the acquired six modes of each signal were calculated. The energy distributions of the 30 sets of signals are listed in Table 2. The energy of the rock fracturing signals is in the low-frequency region, whereas the energy of the blasting vibration signals is the high-frequency region.

The normalized energy of the 15 sets of rock fracturing signals in each mode is shown in Figure 7 and that of the 15 sets of blasting vibration signals in each mode is shown in Figure 8. Clearly, the decomposed rock fracturing signals have their energy distribution mainly concentrated in the modes $u_4$, $u_5$, and $u_6$ and the energy in these modes is 94.65% of the total energy. The decomposed blasting vibration signals have their distribution concentrated in the modes $u_1$, $u_2$, and $u_3$ and the energy in these modes is 83.21% of the total energy; the energy distribution of the other modes is the energy of the interference noise in the signal. Clearly, there are differences in the energy distribution of the rock fracturing and blasting vibration signals of each mode.

**Table 2 Normalized energy distribution of the rock fracturing and blasting vibration signals**

| No. | Rock fracturing signal (%) | | | | | | $C_x$ | No. | Blasting vibration signal (%) | | | | | | $C_x$ |
|---|---|---|---|---|---|---|---|---|---|---|---|---|---|---|---|
| | $P(1)$ | $P(2)$ | $P(3)$ | $P(4)$ | $P(5)$ | $P(6)$ | | | $P(1)$ | $P(2)$ | $P(3)$ | $P(4)$ | $P(5)$ | $P(6)$ | |
| 1 | 1.03 | 4.57 | 1.29 | 56.14 | 33.76 | 3.21 | 0.71 | 1 | 12.49 | 62.88 | 10.15 | 6.18 | 5.52 | 2.78 | 0.40 |
| 2 | 0.02 | 0.09 | 3.04 | 1.53 | 13.2 | 82.12 | 0.96 | 2 | 6.92 | 64.93 | 7.11 | 15.34 | 1.72 | 3.98 | 0.42 |
| 3 | 0.75 | 4.68 | 3.55 | 8.37 | 80.0 | 2.65 | 0.78 | 3 | 9.59 | 64.79 | 15.01 | 5.09 | 3.83 | 1.69 | 0.39 |
| 4 | 1.42 | 8.41 | 2.11 | 47.28 | 37.38 | 3.40 | 0.70 | 4 | 56.48 | 23.23 | 13.17 | 2.77 | 0.91 | 3.44 | 0.30 |
| 5 | 0.04 | 0.13 | 0.08 | 5.25 | 12.18 | 82.32 | 0.96 | 5 | 34.65 | 45.30 | 10.02 | 5.11 | 1.39 | 3.53 | 0.34 |
| 6 | 0.39 | 1.82 | 1.00 | 57.28 | 12.35 | 27.16 | 0.77 | 6 | 16.35 | 54.80 | 11.65 | 8.66 | 1.80 | 6.74 | 0.41 |
| 7 | 1.10 | 4.53 | 4.77 | 16.12 | 28.45 | 45.03 | 0.84 | 7 | 0.36 | 2.96 | 71.43 | 11.65 | 7.09 | 6.51 | 0.57 |
| 8 | 0.35 | 0.89 | 0.44 | 33.23 | 47.91 | 17.18 | 0.80 | 8 | 29.80 | 40.16 | 7.05 | 15.26 | 5.65 | 2.08 | 0.39 |
| 9 | 1.42 | 8.41 | 2.11 | 47.28 | 37.38 | 3.40 | 0.70 | 9 | 0.31 | 43.12 | 40.29 | 12.93 | 0.64 | 2.71 | 0.46 |
| 10 | 0.51 | 1.54 | 0.38 | 30.26 | 18.06 | 49.25 | 0.85 | 10 | 7.75 | 43.95 | 19.04 | 15.13 | 4.97 | 9.16 | 0.49 |
| 11 | 0.56 | 3.19 | 0.78 | 65.03 | 20.66 | 9.78 | 0.72 | 11 | 7.13 | 17.45 | 63.64 | 8.82 | 2.28 | 0.68 | 0.47 |
| 12 | 0.87 | 4.37 | 1.36 | 66.47 | 9.53 | 17.40 | 0.72 | 12 | 3.50 | 34.85 | 45.71 | 8.02 | 7.33 | 0.59 | 0.47 |
| 13 | 0.34 | 0.89 | 0.44 | 33.04 | 48.20 | 17.09 | 0.80 | 13 | 1.11 | 1.43 | 76.49 | 13.74 | 5.70 | 1.53 | 0.54 |
| 14 | 0.92 | 3.00 | 0.85 | 67.20 | 16.27 | 11.76 | 0.72 | 14 | 2.50 | 26.81 | 59.22 | 9.13 | 1.37 | 0.97 | 0.47 |
| 15 | 0.01 | 0.01 | 0.28 | 0.29 | 9.40 | 90.01 | 0.98 | 15 | 8.84 | 42.30 | 31.29 | 10.08 | 4.27 | 3.22 | 0.45 |

In Figure 7, the open circles denote the center of the energy distribution plane of the 15 sets of rock fracturing signals of the energy distribution plane, respectively. The solid circles in Figure 8 denote the center of the 15 sets of blasting vibration signals. After setting the initial threshold $T_{ini} = 0.56$, the decision stump algorithm was applied to the 30 signal sets and the optimal classification identification threshold was determined at $T_{best} = 0.58$.

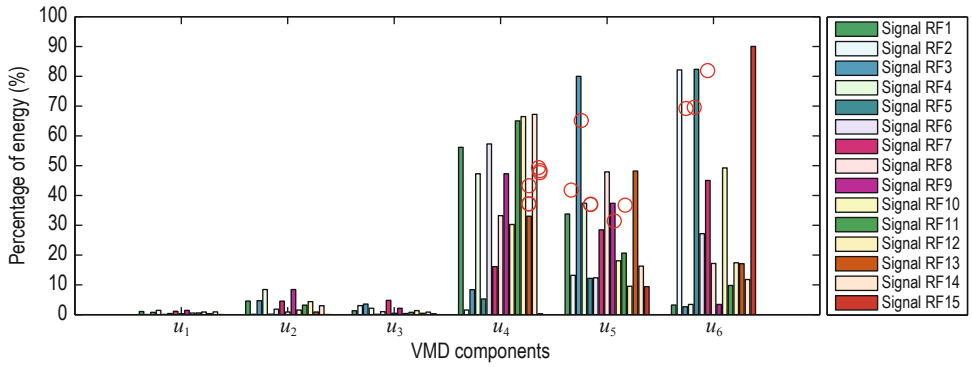


**Fig.7 Energy distribution of the 15 sets of rock fracturing (RF) signals.**

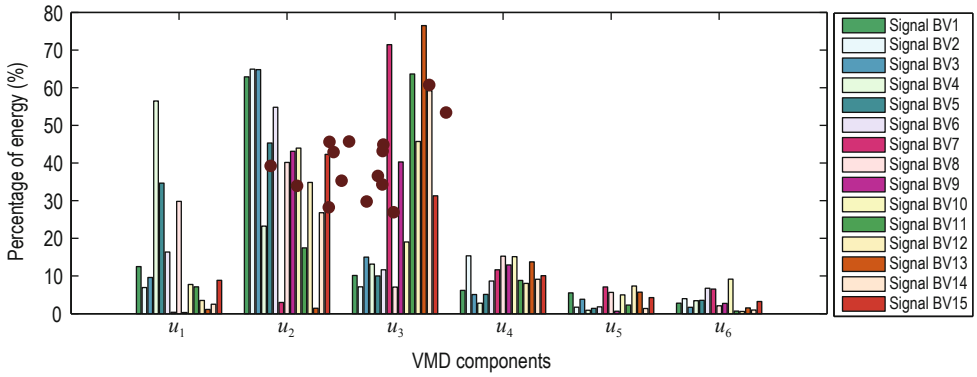


**Fig.8 Energy distribution of the 15 sets of blasting vibration (BV) signals.**

In this study, 20 sets of coal-rock fracturing and blasting vibration signals were selected for testing. Then, the energy centers of each set of the microseismic signals were calculated and those with horizontal coordinates were normalized as the energy focus coefficient of the X-axis $C_x$, as shown in Figure 9, in which the 20 solid circles denote the energy focus coefficients of the blasting vibration signals and the 20 open circles denote the energy focus coefficients of the rock fracturing signals. The signals were classified according to the optimal identification threshold $T_{best}$ = 0.58. Out of 20 sets of microseismic signals, only one set of blasting vibration signals was misclassified as rock fracturing microseismic signal and all 20 sets of coal-rock fracturing microseismic signals were correctly identified. The proposed method is highly accurate and could replace or assist manual identification. Adding the test data to the training group can update the optimal identification threshold.

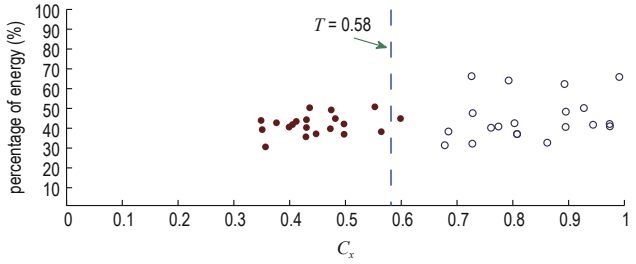


**Fig.9 Classification of the microseismic signals.**

The VMD method, EMD decomposition, and wavelet packet decomposition were used to identify 100 sets of coal-rock fracturing microseismic signals and 100 sets of blasting vibration signals. The method accuracies are shown in Table 3. Clearly, the proposed method is the most accurate.

**Table 3 VMD, EMD, and wavelet packet accuracy**

| Identification method | Accuracy (%) | |
|---|---|---|
| | 100 sets of coal-rock fracturing signals | 100 sets of blasting vibration signals |
| VMD | 98% | 97% |
| EMD | 92% | 87% |
| Wavelet packet | 94% | 96% |

# Conclusions

The VMD decomposition method is used to analyze coal-rock fracturing and blasting vibration signals. VMD can achieve the effective separation of the signal frequency domain and components, yielding more accurate energy distribution eigenvalue of the signal in each frequency band.

There is significant difference in the energy distribution between the microseismic signals of rock fracturing and blasting vibration. The energy of the rock fracturing signals is mainly concentrated in the low-frequency modes, whereas the energy of the blasting vibration signals is mainly concentrated in the three high-frequency modes.

The energy distribution eigenvector of the signals is used to identify the coal-rock and blasting vibration signals. The energy distribution center coefficient obtained from the dimension reduction of the energy distribution eigenvector is used to classify and identify the two kinds of microseismic waves, with accuracy of 97.5% or better.

Clearly, the proposed method can be successfully applied to identify rock fracturing and blasting vibration signals.

# Acknowledgements

We wish to thank the reviewers for their constructive comments.

# References

Akaike, H., 1971, Information theory and an extension of the maximum likelihood principle: 2nd International Symposium on Information Theory, 267−281.

Allen, R. V., 1978, Automatic earthquake recognition and timing from single traces: Bull.seism.soc.am, **68**(5), 1521−1532.

Alvanitopoulos, P. F., Papavasileiou, M., Andreadis, I., and Elenas, A., 2012, Seismic intensity feature construction based on the Hilbert-Huang transform: IEEE Transactions on Instrumentation and Measurement, **61**(2), 326−337.

Allmann, B. P., Shearer, P. M., and Hauksson, E., 2008, Spectral discrimination between quarry blasts and earthquakes in Southern California: Bulletin of the Seismological Society of America, **98**(4), 2073−7079.

Dong, L. J., Wesseloo, J., Potvin, Y., and Li, X., 2016, Discrimination of mine seismic events and blasts using the fisher classifier, naive Bayesian classifier and logistic regression: Rock Mechanics and Rock Engineering,

**49**(1), 183−211.

Gaci, S., 2014, The use of wavelet-based denoising techniques to enhance the first-arrival picking on seismic traces: IEEE Transactions on Geoscience and Remote Sensing, **52**(8), 4558−4563.

Huang, H. M., Bian, Y. J., Lu, S. J., Jiang, Z. F., and Li, R., 2010, A wavelet feature research on seismic waveforms of earthquakes and explosions: Acta Seismologica Sinica, **32**(3), 270−276.

Huang, N. E., Shen, Z., Long, S. R., Wu, M. C., Shih, H. H., and Zheng, Q., 1998, The empirical mode decomposition and Hilbert spectrum for nonlinear and nonstationary time series analysis: Proceedings of the Royal Society A Mathematical Physical & Engineering Sciences, **454**(1971), 903−995.

Jiang, F. X., Yin, Y. M., Zhu, Q. J., Li, S. X., and Yu, Z. X., 2014, Feature extraction and classification of mining microseismic waveforms via multi-channels analysis: Journal of China Coal Society, **39**(2), 229−237.

Jia, R. S., Zhao, T. B., Sun, H. M., and Yan, X. H., 2015, Micro-seismic signal denoising method based on empirical mode decomposition and independent component analysis: Chinese Journal of Geophysics, **58**(3), 1013−1023. doi:10.6038/CJG20150326

Jia, R. S., Sun, H. M., Peng, Y. J., Liang, Y. Q., and Lu, X. M., 2016, Automatic event detection in low SNR microseismic signals based on multi-scale permutation entropy and a support vector machine: Journal of Seismology, **21**(4), 1−14.

Konstantin, D., and Dominique, Z., 2014, Variation mode decomposition: IEEE Transactions on Signal Processing, **62**(3), 531−544.

Lu, C. P., Dou, L. M., Wu, X. R., Wang, H. M., and Qin, Y. H., 2005, Frequency spectrum analysis on microseismic monitoring and signal differentiation of rock material: Chinese Journal of Geotechnical Engineering, **27**(7), 772 −775.

Liu, X. Q., Shen, P., Zhang, L., and Li, Y. H., 2003, Using method of energy linearity in wavelet transform to distinguish explosion or collapse from nature earthquake: Northwestern Seismological Journal, **25**(3), 204−209.

Ma, J., Zhao, G. Y., Dong, L. J., Chen, G. H., and Zhang, C. X., 2015, A comparison of mine seismic discriminators based on features of source parameters to waveform characteristics: Shock and Vibration, 2015(1), 1−10.

Shang, X. Y., Li, X. B., Peng, K., Dong, L. J., and Wang, Z. W., 2016, Feature extraction and classification of mine microseism and blast based on EMD_SVD: Chinese Journal of Geotechnical Engineering, **38**(10), 1849−1858.

Tang, S. F., Tong, M. M., Pan, Y. X., He, X. M., and Lai, X. S., 2011, Energy spectrum coefficient analysis of wavelet features for coal rupture microseismic signal: Chinese Journal of Scientific Instrument, **32**(7), 1522−1527.

Tang, G. J., and Wang, X. L., 2015, Parameter optimized variational mode decomposition method with application to incipient fault diagnosis of rolling bearing: Journal of Xi'an JiaoTong University, **49**(5), 73−81.

Wang, B. L., 2018, Automatic pickup of arrival time of channel wave based on multi-channel constraints: Applied Geophysics, **15**(1), 118−124.

Wu, X., Qian, J. S., Wang, H. Y., and Qin, H. C., 2014, Study on multi-scale nonlinear feature extraction and signal identification for microseismic signal: Chinese Journal of Scientific Instrument, **35**(5), 969−975.

Xie, P., Yang, F. M., Li, X. X., Yang, Y., Chen, X. L., and Zhang, L. T., 2016, Functional coupling analyses of electroencephalogram and electromyogram based on variational mode decomposition-transfer entropy: Acta Physica Sinica, **65**(11), 11870−1:9.

Zhu, Q. J., Jiang, F. X., Yu, Z. X., Yin, Y. M., and Lu, L., 2012a, Study on energy distribution characters about blasting vibration and rock fracture microseismic signal: Chinese Journal of Rock Mechanics and Engineering, **31**(4), 723−730.

Zhu, Q. J., Jiang, F. X., Yin, Y. M., Yu, Z. X., and Wen, J. L., 2012b, Classification of mine microseismic events based on wavelet-fractal method and pattern recognition: Chinese Journal of Geotechnical Engineering, **34**(11), 2036−2042.

Zhao, G. Y., Ma, J., Dong, L. J., Li, X. B., and Chen, G. H., 2015, Classification of mine blasts and microseismic events usingstarting-up features in seismograms: Transactions of Nonferrous Metals Societyof China, **25**(10), 3410−3420.

Zhang, M., Zhu, Y. L., Zhang, N., and Zhang, Y. Y., 2016, Feature extraction of transformer partial discharge signals based on varitional mode decomposition and multi-scale permutation entropy: Journal of North China Electric Power University, **43**(6), 31−37.

Zhang, X. L., Lu, X. M., Jia R. S., and Kan, S. T., 2018, Micro-seismic signal denoising method based on variational mode decomposition and energy entropy: Journal of China Coal Society, **43**(2), 356−363.

**Zhang Xing-Li** received her B.Eng. (2002) and M.Eng. (2005) in Software Engineering from the Taiyuan University of Technology, and her Ph.D. (2010) in Software Engineering from Shandong University of Science and Technology. She is presently working in the College of Computer Science and Engineering, Shandong University of Science and Technology. Her main research interests are microseismic signal analysis and processing.